



The very hard and the very soft: Modeling bio-inspired scaled skins using the discrete element method

Ali Shafiei^a, J. William Pro^a, Roberto Martini^a, Francois Barthelet^{a,b,*}

^a Department of Mechanical Engineering, McGill University, 817 Sherbrooke Street West, Montreal, QC H3A 2K6, Canada

^b Department of Mechanical Engineering, University of Colorado, 427 UCB, 1111 Engineering Dr, Boulder, CO 80309, United States

ARTICLE INFO

Keywords:

Bioinspiration
Discrete element method
Segmented hard material
Penetration resistance
Flexural compliance

ABSTRACT

Natural protective systems are attracting an increasing amount of attention for their ability to provide simultaneous flexibility and puncture resistance by combining hard and soft materials in mechanically efficient ways. In typical flexible natural armors, a continuous layer of soft material is either covered or embedded with segmented hard scales. The interaction between the hard scales and the softer surrounding materials give rise to unusual and attractive mechanisms which are not fully understood to this day. Here we propose and validate the discrete-element method (DEM) to capture the mechanics of stiff scales on soft substrates including scale-substrate elastic deformations, scale-scale interaction through the substrate, and direct scale-scale interaction by contact. We considered two configurations: (i) hard scales on soft substrates to capture scale tilting and penetration resistance, and (ii) hard scales on soft membranes to study flexural compliance. The computational efficiency of the DEM algorithm allowed for large parametric studies with many combinations of aspect ratio, slant angle, and gap size to identify the best designs in terms of resistance to unstable tilting, coverage, penetration resistance, and flexural compliance. DEM is a promising tool for the design and optimization of fish-skin-like protective structures, also providing new insights into the synergistic role of the hard scales and the soft substrate.

1. Introduction

Modern engineering applications are requiring lighter, stronger, tougher, and multifunctional materials. In this quest for better engineering materials, nature can provide outstanding models and inspiration for new designs. Natural materials have high mechanical performance, can produce seemingly mutually exclusive properties (Ritchie, 2011), and are inherently multifunctional (Wegst et al., 2014). A powerful paradigm in structural biological materials is the combination of hard and soft materials in well-controlled micro-architectures (Wegst et al., 2014; Barthelet, 2015; Martini et al., 2017; Rajabi et al., 2016; Porter et al., 2013; Yang et al., 2013; Rajabi et al., 2016). Scaled natural flexible armors (Fig. 1) are excellent examples of this concept: They combine hard materials (mineralized collagen, dry keratin) with soft materials which are orders of magnitude more compliant (Chintapalli et al., 2014; Martini and Barthelet, 2016). Natural scaled armors combine two properties which are typically mutually exclusive: high surface hardness for protection against puncture or laceration, combined with high flexural compliance for fast locomotion. In fish skins the

* Corresponding author at: Department of Mechanical Engineering, University of Colorado, 427 UCB, 1111 Engineering Dr, Boulder, CO 80309, United States.

E-mail address: francois.barthelet@colorado.edu (F. Barthelet).

<https://doi.org/10.1016/j.jmps.2020.104176>

Received 7 April 2020; Received in revised form 3 August 2020; Accepted 3 October 2020

Available online 5 October 2020

0022-5096/© 2020 Published by Elsevier Ltd.

hard scales are attached to a soft substrate (Fig. 1a and b). Under flexural deformation the scales can glide on one another, providing high compliance to the system (Funk et al., 2015; Rudykh et al., 2015; Vernerey and Barthelat, 2014). Moreover, interactions between neighboring scales can improve the penetration resistance (Vernerey and Barthelat, 2010), and distribute the localized puncture force over a larger area to prevent excessive strains in the underlying tissues, thereby delaying blunt injuries (Martini and Barthelat, 2016; Zhu et al., 2013; Browning et al., 2013). Experiments on synthetic scaled systems made of hexagonal glass plates on elastomeric substrates showed that discrete glass plates not only provide flexural compliance to the system, but also increase puncture resistance by up to 70% compared to a continuous glass layer (Chintapalli et al., 2014). Decreasing the size of the plates reduces their flexural span which delays fracture up to a point where the scales are small enough to tilt from the action of the sharp indenter (Chintapalli et al., 2014; Martini and Barthelat, 2016; Martini and Barthelat, 2016). The tilting of individual plates is indeed an important failure mode in scaled skin which is prominent in animals with very hard scales such as in alligator gar (Martini and Barthelat, 2016). A mechanical criterion was recently proposed for the tilting and instability of hard plates on a soft substrate (Martini and Barthelat, 2016). Experiments on 3D printed scales have later suggested that the indented scale can be stabilized by neighboring scales, and that scale geometry and arrangement have a deep impact on this mechanism (Martini et al., 2017). Despite these recent advances, the mechanics of scaled skins is still not fully understood. For example, how scales interact during flexural deformation and puncture, how they distribute concentrated forces over wide areas, and how the geometry and arrangement of the scales govern mechanical performance are important effects that are not fully understood.

Some insights can be provided from experiments on synthetic scales (Martini et al., 2017, Chintapalli et al., 2014, Connors et al., 2019), also from finite element modeling such as a 2D simulation of a scale-covered substrate under blunt indentation loading (Browning et al., 2013), and a 3D flexural modeling of a system of hard scales on a soft membrane (Vernerey et al., 2014). But in the both finite element models, a limited number of scales were used. The large number of contact regions occurring concurrently are difficult to properly capture with standard numerical methods such as finite elements where convergence is difficult (if at all possible). In this article, we propose the discrete element method (DEM) as an approach to model the deformation of scaled skins, including multiple scale-scale interactions. The discrete element method (DEM) offers a computationally efficient alternative to the conventional finite element method (FEM) by reducing the degrees of freedom in the problem (Dugué et al., 2013). DEM is also well suited for the systems containing a large number of rigid elements with complex interaction laws (Dugué et al., 2013; Pro et al., 2015; Bolander and Saito, 1998; Abid et al., 2018; Abid et al., 2019; Lim et al., 2015; Pro et al., 2015; Pro and Barthelat, 2019; Pro and Barthelat, 2020). For instance, we recently used DEM on nacre which had a structure similar to fish skin: both are made of hard plates connected by much softer material (Abid et al., 2018, Abid et al., 2019). After validation of this numerical tool, we used DEM to explore the design space of a large number (720) of scale-covered systems with interesting combinations of puncture resistance and flexibility.

2. Discrete element method (DEM) for scales: formulation and validation

For this study we developed a 2D DEM model of hard scales perfectly bonded onto a soft substrate (Fig. 2a). The scales were identical and modeled as parallelograms defined by a thickness t , length $2L$, and slant angle α . The bases of the scales were assumed to be perfectly bonded to a soft substrate and uniformly spaced, with a gap distance d . To model puncture, a concentrated force was applied on the upper face of the middle scale along the direction normal to the surface of the substrate (Fig. 2a), while the substrate was

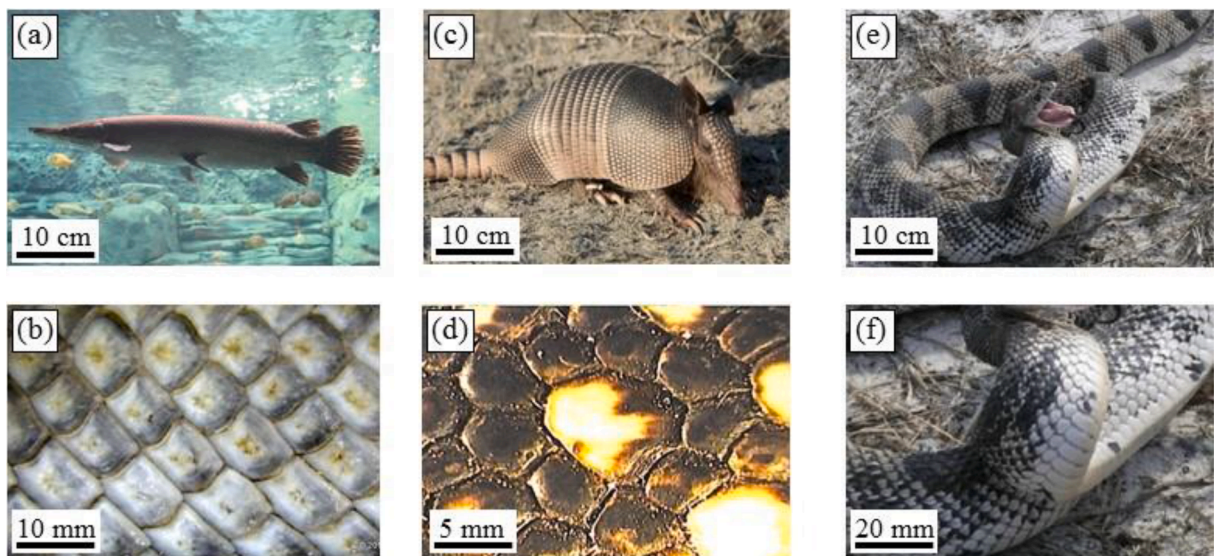


Fig. 1. Examples of animals with armors made of combinations of segmented hard elements and soft materials together: (a)-(b) alligator gar (*Atractosteus spatula*, adapted from Nelson, 2014); (c)-(d) Armadillo (*Dasypus novemcinctus*, adapted from (Chen et al., 2011; Garst and Garst, 1985)); (e)-(f) Northern pine snake (*Pituophis melanoleucus*, adapted from Burger and Zappalorti, 2011).

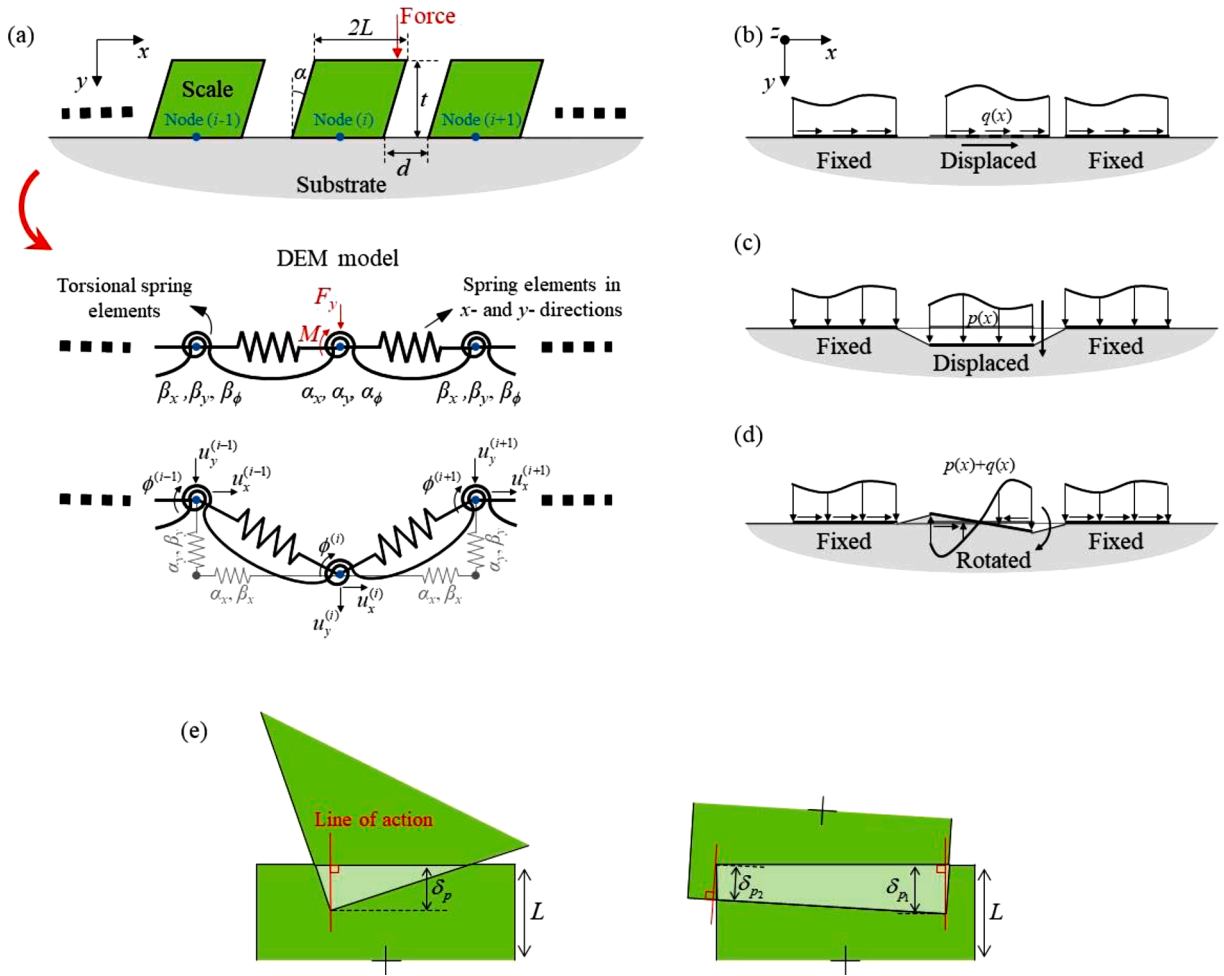


Fig. 2. (a) The system of hard scales attached to a soft substrate, The DEM model in which the substrate is replaced by spring elements in the x- and y-directions, and torsional spring elements; The distribution of the shear load $q(x)$ and the normal load $p(x)$ for the models with (b) a horizontal displacement boundary condition (the surfaces at the sides are fixed, and the middle one is displaced); (c) a vertical displacement boundary condition (the surfaces at the sides are fixed, and the middle one is displaced); (d) applying a rotation boundary condition (the surfaces at the sides are fixed, and the middle one is rotated) which makes both the shear and normal loads on the surfaces ($q(x) + p(x)$); (e) Intersection of two scales with a triangle shape which makes a force along the line of action (the red line), or with a four sided shape which makes two separate forces along their line of actions (the red lines) (For interpretation of the references to color in this figure legend, the reader is referred to the web version of this article.).

modeled as a half-space. The position of each scale was represented by a node coinciding with the midpoint of the lower side of the scale. Each of the nodes has three degrees of freedom: translations in the x- and y-directions, and rotation about the z-axis. The substrate was modeled as a linear elastic half-space (modulus E_s , Poisson's ratio ν) with small strains. The scales were assumed to be several orders of magnitude stiffer than the substrate (Zhu et al., 2012), and therefore we modeled the scales as rigid for the purpose of efficiently capturing scale-substrate interactions (scale-scale interactions were captured using a simplified contact model that takes in account the deformability of the scale, as detailed below). For simplicity the substrate was modeled with spring elements (Fig. 2a) that captured not only the reaction of the substrate onto individual scales, but also the elastic coupling between neighboring scales. More specifically, the two reaction forces and the reaction moment from the substrate to the individual scales were captured with three "direct" stiffness coefficients α_x, α_y and α_ϕ , and the effect of the neighboring scales on a given scale were captured with another three "coupling" coefficients β_x, β_y and β_ϕ . The forces (F_x, F_y) and the moment M_z (about the z axis) on the ith node were expressed as:

$$\begin{cases} F_x^{(i)} = \frac{E_s L t}{(1-\nu^2)} \left(\alpha_x \frac{u_x^{(i)}}{t} - \beta_x \left(\frac{u_x^{(i-1)}}{t} + \frac{u_x^{(i+1)}}{t} \right) \right) \\ F_y^{(i)} = \frac{E_s L t}{(1-\nu^2)} \left(\alpha_y \frac{u_y^{(i)}}{t} - \beta_y \left(\frac{u_y^{(i-1)}}{t} + \frac{u_y^{(i+1)}}{t} \right) \right) \\ M_z^{(i)} = \frac{E_s L^3}{(1-\nu^2)} (\alpha_\phi \phi^{(i)} - \beta_\phi (\phi^{(i-1)} + \phi^{(i+1)})) \end{cases} \quad (1)$$

Where E_s is the Young's modulus of the substrate, and ν is the Poisson's ratio of the substrate. u_x and u_y are the nodal displacements in the x - and y -directions, respectively, and ϕ is the nodal in-plane rotation. To appreciate the effect of coupling between the scales, consider a simple example where all the scales are clamped, except scale $i+1$ which is displaced by $u_x^{(i+1)} > 0$. Displacing that scale deforms the surrounding substrate, so that a force $F_x^{(i)} < 0$ must be applied onto scale i to keep it immobile (Eq. (1)). To calibrate the coefficients α_x , α_y , α_ϕ , β_x , β_y and β_ϕ we used Boussinesq's and Cerruti's close-form solution for the substrate as an elastic half-space where we assumed that the substrate is adequately thick (Barber, 2002; Okumura, 1995). For the case of thin substrate assumption, other theories are available to be used which is beyond the scope of this work (Wu and Ru, 2019; Lin et al., 2008; Li and Dai, 2020). We considered three scales on the elastic half-space, first subjecting the middle scale to a tangential displacement u_x (Fig. 2b) while the other two scales were clamped.

The relation between the tangential displacement u_x and the horizontal (x -direction) distributed shear load $q(\zeta, \gamma)$ on the surface of the substrate underneath the scales (Fig. 2b) is given as:

$$u_x = \frac{1+\nu}{\pi E_s} \iint q(\zeta, \gamma) \left[\frac{1-\nu}{\sqrt{(x-\zeta)^2 + (z-\gamma)^2}} + \frac{\nu(x-\zeta)^2}{\sqrt{((x-\zeta)^2 + (z-\gamma)^2)^3}} \right] d\zeta d\gamma \quad (2)$$

Where z is the out-of-plane direction. We obtained the distributed shear load $q(x, z)$ from Eq. (2), which we then integrated over the area of the scales to obtain the shear force for each scale. Dividing the shear forces on the middle scale, and on the neighbouring scales by the imposed displacement of the middle scale (u_{x0}) provided the stiffness coefficients α_x and β_x , respectively. The process was repeated for a normal displacement u_y (Fig. 2c) where we imposed a displacement u_{y0} to the middle scale. To compute α_y and β_y we used the equation:

$$u_y = \frac{1-\nu^2}{\pi E_s} \iint p(\zeta, \gamma) \frac{1}{\sqrt{(x-\zeta)^2 + (z-\gamma)^2}} d\zeta d\gamma \quad (3)$$

Where $p(\zeta, \gamma)$ is the distributed normal load in the vertical (y) direction on the surface of the substrate below the scales Fig. 2c). Finally, we imposed a rotation ϕ_0 on the middle scale by still keeping the other two scales clamped (Fig. 2d). Using Eqs. (2) and (3), we obtained the distributed shear and normal loads and the resultant moment on each scale. The coefficients α_ϕ and β_ϕ were computed by dividing the moment on the middle and neighbouring scales (respectively) by the imposed rotation on the middle scale ϕ_0 . The coefficients α_x , α_y , α_ϕ , β_x , β_y and β_ϕ are expressed as

$$\begin{cases} \alpha_x = \frac{\iint_{A_m} q(x, z) dx dz}{u_{x0}} \quad , \quad \beta_x = \frac{\iint_{A_n} q(x, z) dx dz}{u_{x0}} \\ \alpha_y = \frac{\iint_{A_m} p(x, z) dx dz}{u_{y0}} \quad , \quad \beta_y = \frac{\iint_{A_n} p(x, z) dx dz}{u_{y0}} \\ \alpha_\phi = \frac{\iint_{A_m} [q(x, z)(x-x_m)\sin\phi_0 + p(x, z)(x-x_m)\cos\phi_0] dx dz}{\phi_0} \\ \beta_\phi = \frac{\iint_{A_n} [q(x, z)(x-x_n)\sin\phi_0 + p(x, z)(x-x_n)\cos\phi_0] dx dz}{\phi_0} \end{cases} \quad (4)$$

In which A_m and A_n are the areas of the middle scale and either of the neighbouring scales, respectively. x_m and x_n are the x -coordinates of the midpoint of the lower side of the middle scale and either of the neighbouring scales, respectively. An important implication of this result is that individual scales can interact with their neighbors not necessarily only by direct contact but also through deformations in the substrate. Direct contact between the scales is another feature of the model which is critical to capture puncture and flexural deformations. In our model the contacting scales were assumed to be rigid and frictionless, and we used a simple yet accurate and computationally efficient contact algorithm inspired by the Winkler elastic foundation model (Johnson, 1987). We first used shape intersection algorithms to detect collision between pairs of scales, and we used kinematics to compute the penetration

distance δ_p (Fig. 2e) between the contacting scales. The contact force was then computed from δ_p using:

$$\frac{F_{ct}}{LbE_{ct}} = C_1 \left(\frac{\delta_p}{L}\right)^{C_2} \tag{5}$$

Where E_{ct} is the contact modulus, and b is the out-of-plane dimension (width) of the scales. The calibration constants C_1 and C_2 were obtained using a 2D finite element model (ANSYS V16 2016, PA, US) in which the corner of one scale penetrated into the edge of another scale under controlled displacement (Fig. 2e). From the finite element calculations we computed the resultant contact force (the interfaces were assumed to be frictionless) and determined $C_1 = 1.1$ and $C_2 = 0.23$. We also defined the line of action of F_{ct} so that it is intersecting the penetrating corner of one the scales, and is perpendicular to the edge of the other scale (Fig. 2e). For the case of four-sided overlap area (Fig. 2e), we applied the procedure to two instances of corner contact and applied Eq. (5) twice. In addition to forces, direct contact between scales may induce moments about the out-of-plane axis z . We computed the effective nodal moment due the contact forces as:

$$M_{ij} = r_{ct} \times F_{ct,ij} \tag{6}$$

Where M_{ij} is the effective nodal moment induced by scale i onto neighboring scale j , r_{ct} is the position vector of the contact force relative to node i and $F_{ct,ij}$ is the contact force which scale i exerts on scale j . Since the contact model introduces geometrical nonlinearities we used the iterative Newton-Raphson method to obtain numerical solutions (Abid et al., 2018).

To validate our model we performed puncture tests on a system composed of a pair of Acrylonitrile butadiene styrene (ABS) blocks glued onto a softer elastomeric substrate. The blocks were 3D printed with a high resolution Direct Light Projector (DLP) 3D printer (Micro HiRes Machine, EnvisionTech, 2019), which produced fully dense and pore-free blocks. We tested 3D printed ABS along different directions and verified that the blocks were isotropic, with a modulus $E_{ABS} = 3$ GPa. The blocks were then glued onto the surface of a thick polyurethane substrate using cyanoacrylate. The polyurethane we used is four orders of magnitude softer than ABS, with a measured modulus of $E_s = 310$ kPa (we used a Poisson’s ratio $\nu = 0.5$ (Martini et al., 2017)). The assumption of rigid blocks compared to the substrate, required for our DEM simulation, was therefore verified. For the puncture test, a needle was pressed on the upper surface of one of the blocks, which caused the substrate to deform and the blocks to displace and tilt (Fig. 3a).

For validation we compared the force-displacement curves obtained experimentally and through DEM, which showed excellent agreement (Fig. 3b). The model properly captured the initial stiffness of the system and the onset of contact between the blocks. Following contact, the stiffness of the system suddenly increased (which shows as a ‘kink’ on the puncture force-displacement curve in Fig. 3b), a phenomenon that the DEM model also accurately captured.

3. Parametric study and exploration of geometry-puncture resistance relationships

We used the DEM model to systematically explore the effects of scale geometry and arrangement on puncture resistance. In this first study, we focused on parallelogram-shaped scales placed at regular intervals over the softer substrate. Since there is no length scale associated with the elastic deformation, we use non-dimensional geometrical parameters: the aspect ratio of the scales (L/t), the slant angle of the scales (α), and the normalized gap distance between the scales (d/t). Fig. 4 illustrates models with different combinations of these three geometrical parameters, showing that this approach covered a wide range of possible scale designs.

A first inspection reveals that some designs do not provide adequate coverage, leaving the substrate directly exposed to outside mechanical threats. This issue occurs for all designs with no slant angle ($\alpha = 0$), and more generally when the spacing of the scale is too large and/or the slant angle is too low. On the other hand, designs providing good coverage involve neighboring scales that overlap. To characterize the extent of coverage for each design we defined a non-dimensional coverage parameter $\lambda = t_s/t$ where t is the thickness of the scales, and t_s is obtained by first drawing a vertical line from the upper right corner of a scale. t_s then was computed as the sum of

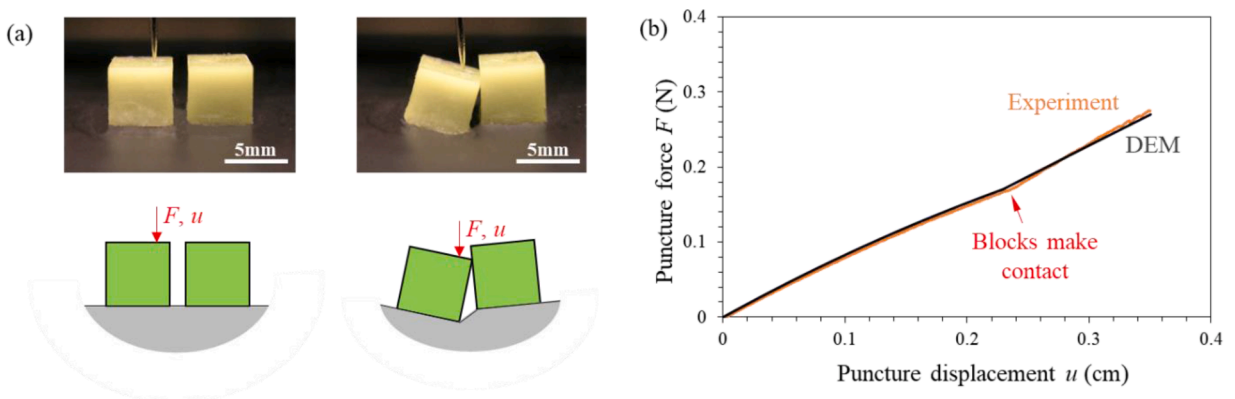


Fig. 3. (a) Experimental and DEM puncture tests on a pair of ABS blocks on a polyurethane substrate; (b) Force-displacement curve showing a good agreement between the experimental and DEM results.

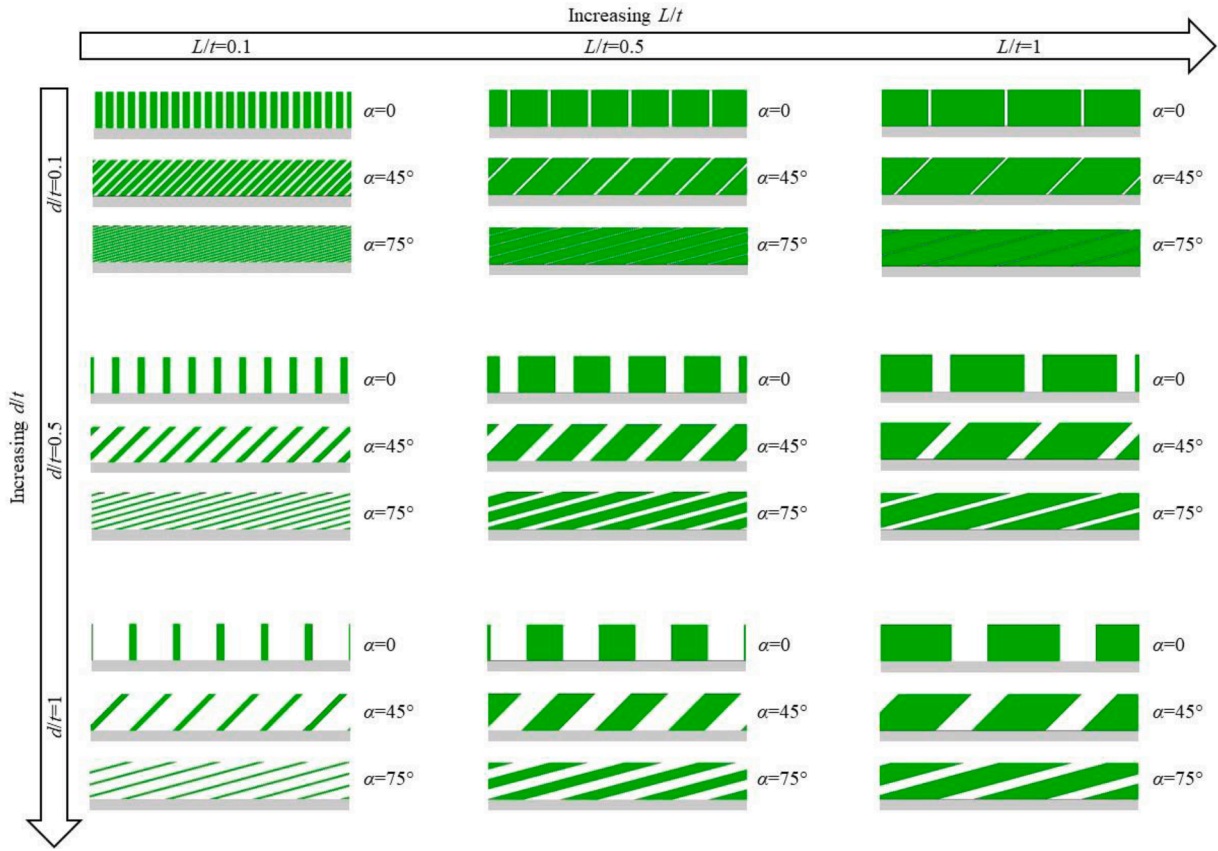


Fig. 4. Models with different combinations of scale gaps (d/t), aspect ratios (L/t) and slant angles (α).

the intersect lengths between that line and the neighboring scales (Fig. 5). By this measure, λ ranges from $\lambda = 0$ (no coverage) to $\lambda = 1$ (full coverage).

For all models, we imposed a vertical force on the upper right corner of the middle scale so that the force applied the largest possible tilting moment on the scale, which represented the “worst-case scenario” for loading. We first present the effect of each parameter on the puncture force-displacement curves (Fig. 6). For all results, we normalized the applied force on the middle scale as $F^* = F(1 - \nu^2) / E_s L t$ (consistent with equation (1)) and the displacement of the punctured point as $u^* = u/t$. Fig. 6a shows the effect of the slant angle α on the deformation of the system for a fixed aspect ratio of $L/t = 1$ and gap of $d/t = 0.1$. Initially, the imposed force simultaneously pushes the scales into the substrate and increases the tilt angle. At the initial stage the puncture stiffness is relatively low, especially at larger slant angles (Fig. 6b) because of the larger moment arm of the applied force. At some point during the simulation the scales start contacting each other (on the snapshots of Fig. 6a, the contact areas are marked in red and on the puncture force-displacement curves in Fig. 6b a (\times) symbol marks every new contact event). For the cases of $\alpha = 0^\circ$ and $\alpha = 45^\circ$ the punctured scale contacts with the neighboring scales at about $u/t = 0.08$, which translates into a kink on the force-displacement curve and a stiffer response. For the case of $\alpha = 0^\circ$, the corner of the punctured scale slides on the side of the neighboring scale with little resistance and the contact force between the scales is mostly horizontal. Introducing a slant angle generates a vertical component to the contact force and a much stiffer response (this result is consistent with our previous experimental study on 3D printed scales Martini et al., 2017). For the model with the largest slant angle ($\alpha = 75^\circ$) the initial contact occurs earlier due to the larger tilting moment. The first four contacts do not have a significant effect on the stiffness because of the high tilting moments in the scales. By engaging more scales by contact during loading, the resistance from the contact eventually overcomes the high tilting moment and the stiffness starts increasing. The post-contact stiffness also increases significantly with the scale slant angle. Interestingly, the puncture force can become high enough that additional scales enter contact (Fig. 6a), which distributes the puncture force over an even greater area. Fig. 6c shows the effect of varying the aspect ratio on the response of the system, with a fixed gap of $d/t = 0.1$ and fixed slant angle of $\alpha = 45^\circ$. Larger aspect ratios cause less penetration, but larger tilting moments induced by the loading in the punctured scale, which implies that individual scales offer less resistance to tilting resulting in low initial stiffness (Fig. 6d). In contrast, smaller scales (smaller L/t) penetrate more into the substrate but showed less tilting. This stability effects the post-contact stiffness of the system as well, where the contacting scales with smaller aspect ratios show more resistance against tilting resulting in higher system stiffness (Fig. 6d). Finally, Fig. 6e and 6f show the effect of the gap size for a fixed aspect ratio of $L/t = 0.5$ and slant angle of $\alpha = 45^\circ$. The gap size has no significant effect on the initial stiffness of the systems and little effect on post contact stiffness. The main effect of increasing d/t was to delay scale-scale contact (Fig. 6f).

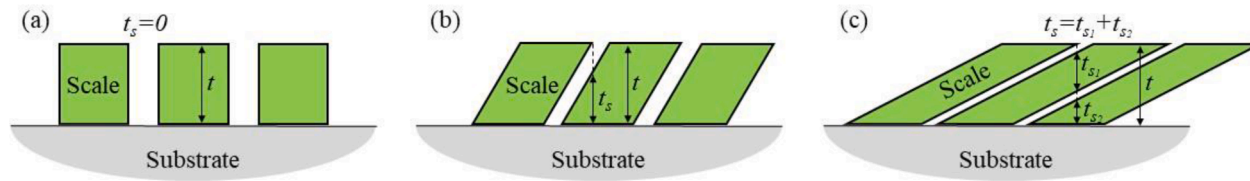


Fig. 5. Diagrams showing three examples on how to compute t_s and $\lambda = t_s/t$. (a) Example with no scale overall and no coverage ($\lambda = 0$); (b) Example with two scales overlapping, leading to intermediate λ ; (c) Example with three scales overlapping, leading to high λ .

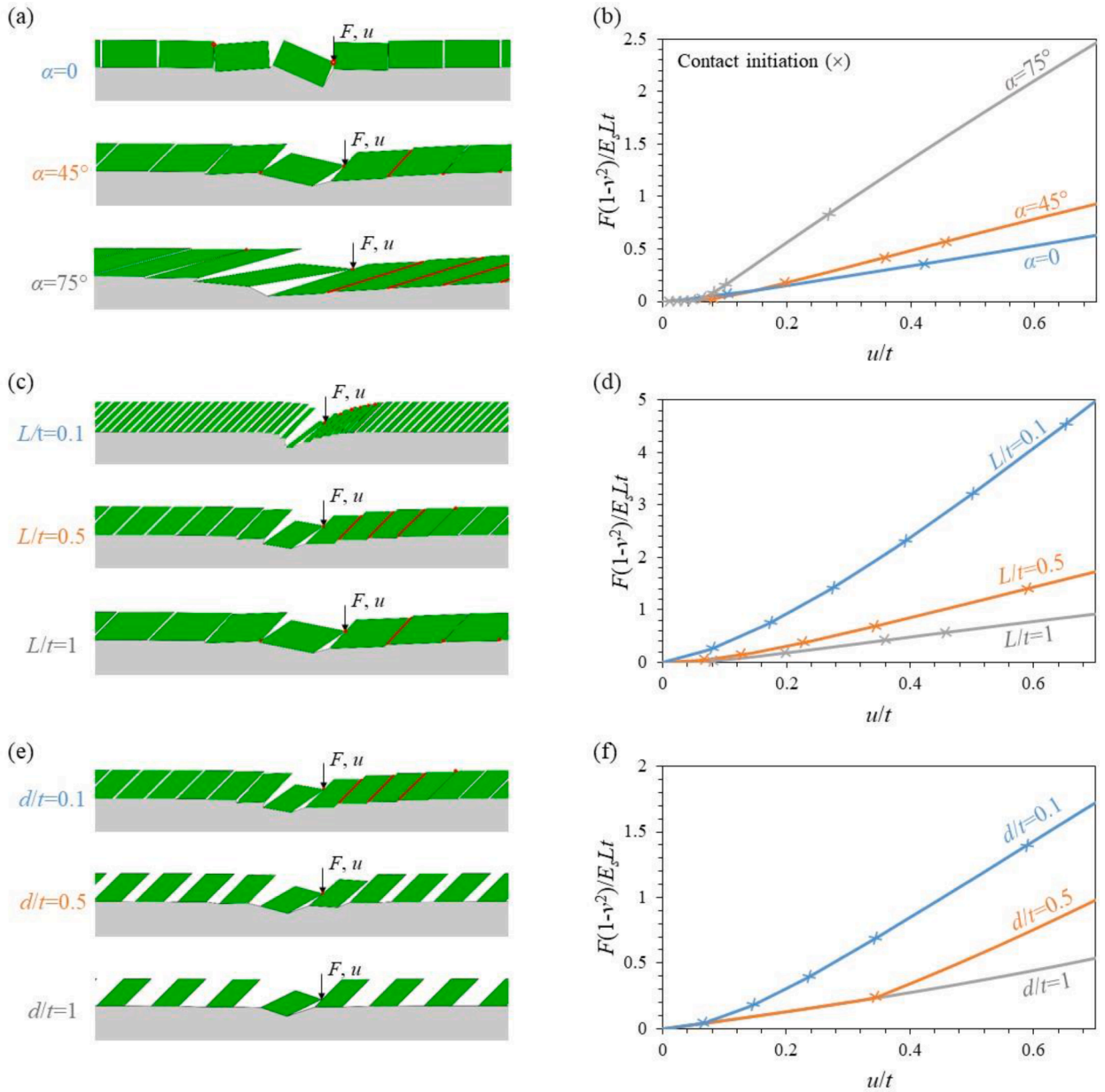


Fig. 6. Deformation of three systems of scales at $u/t=0.7$ on a soft substrate in a puncture test, and the related force-displacement curves: for (a) and (b) a fixed aspect ratio of $L/t=1$ and a gap size of $d/t=0.1$, (c) and (d) a fixed gap size of $d/t=0.1$ and a slant angle of $\alpha=45^\circ$, (e) and (f) a fixed aspect ratio of $L/t=0.5$ and a slant angle of $\alpha=45^\circ$.

In addition to puncture stiffness, we considered the puncture resistance of the scaled surface. There are several possible failure modes for this system, including fracture in the scales, failure of the interface or tearing of the substrate. However, in this study the combination of the materials, geometries and load range was such that we did not observe any of these failure modes. Instead, we focused on a failure mode that occurred by tilting of the indented scale. In this failure mode the indented scale tilts from the action of the needle, and when the tilt reaches a critical angle $\phi_c = \tan^{-1}(\mu)$ (where μ is the friction coefficient between the scale and the needle), the needle suddenly slides on the surface of the tilted scale and finds its way into the substrate (Fig. 7a).

This failure mode was identified on scales from gar fish and duplicated in puncture experiments on 3D printed scales (Martini et al., 2017; Martini and Barthelat, 2016). For each of the models discussed above, we computed a critical force, corresponding to the point where the tilting of the scale reached a critical angle which we took as $\phi_c = 10^\circ$ to be consistent with previous experiments (Martini and Barthelat, 2016). Fig. 7b shows that the gap size, aspect ratio and slant angle, all had a significant effect on the critical force. In general, decreasing the gap between the scales (d/t) increased the critical force, because early contact between the scales increased stability and delayed tilting. Smaller scales (small L/t) were also more stable, because of the reduced lever arm of the applied force. Higher slant

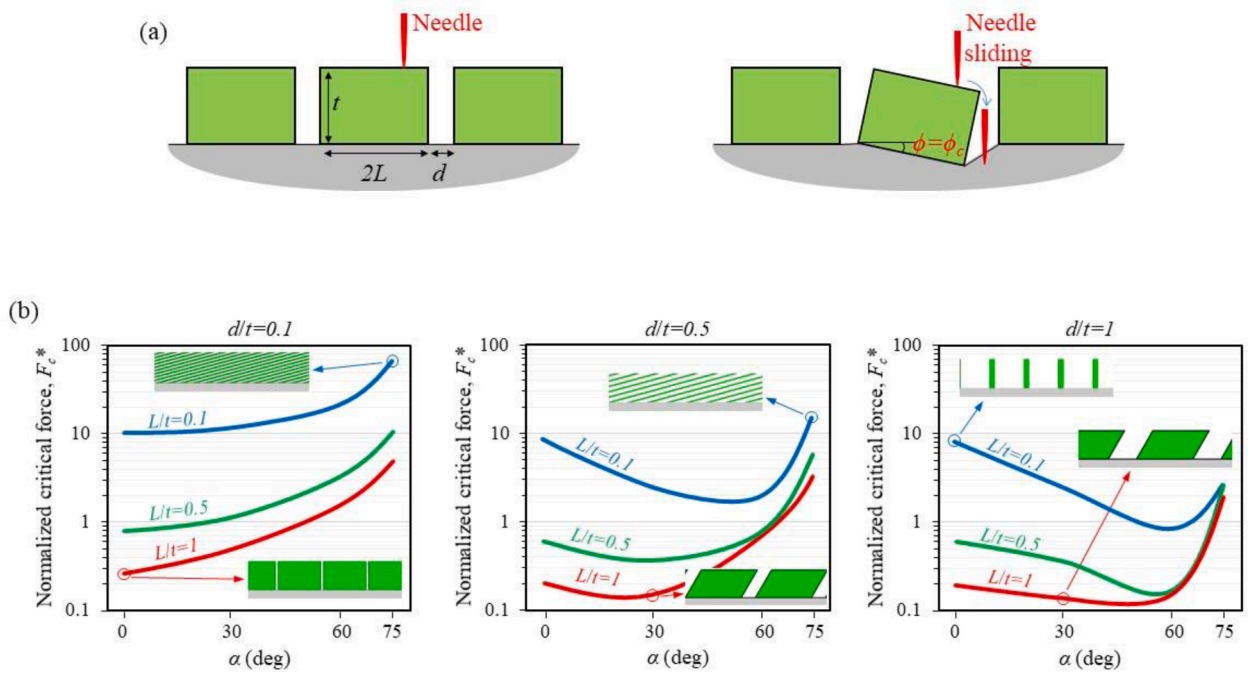


Fig. 7. (a) Reaching the critical angle causes the needle to slide off the scale surface; (b) the effect of the slant angle (α), the aspect ratio (L/t) and the gap (d/t) on the critical force of the system. The critical force is denoted as F_c and is normalized by $F_c^* = F_c (1-\nu^2)/E_sLt$.

angles also increased the critical force as long as the scales contacted early in the puncture process. If the contact was delayed because of a large initial gap between scales, larger slant angles led to larger lever arm for the force and less stability. Compounding all these effects, the smallest aspect ratio ($L/t=0.1$), the smallest gap ($d/t=0.1$) and the largest slant angle ($\alpha=75^\circ$) produced the system with the highest critical force ($F_c(1-\nu^2)/ELt=64$). Fig. 8 maps the puncture stiffness and the critical force for all models of scale designs, showing a strong correlation between these two properties. The highest puncture stiffness was achieved for the case with an aspect ratio of $L/t=0.1$, a slant angle of $\alpha=75^\circ$, and a gap of $d/t=0.1$. This system also has the highest critical force. Among all the design parameters considered here, we found that the slant angle had the most significant effect on the puncture stiffness and critical force.

Contact interaction between scales not only improves critical force, it also improves how the puncture force is distributed onto the substrate (see, for example, Fig. 6a). To better illustrate this effect, Fig. 9 shows the spatial distribution of vertical reaction forces from the substrate onto the scales, for models with different slant angles (under the same puncture force). In the model with no slant angle

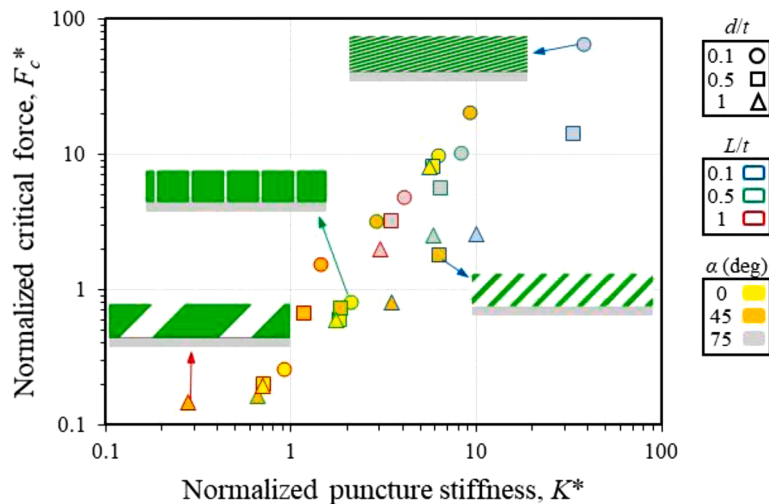


Fig. 8. The relation between the normalized stiffness and the critical force for different combinations of slant angle (α), aspect ratio (L/t) and gap (d/t). The stiffness and critical force are denoted as K and F_c , and are normalized by $K^* = K/E_s t$, and $F_c^* = F_c (1-\nu^2)/E_sLt$, respectively.

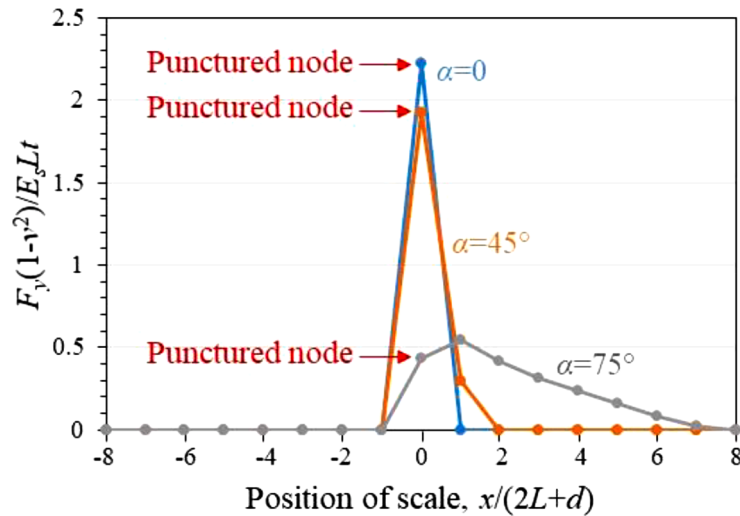


Fig. 9. Force distribution over the models with different slant angles in a puncture test.

($\alpha=0$), only one scale is engaged by the point force, and the force is transmitted to the substrate over a small area. This concentrated distribution could lead to flexural failure of the scale, or damage in the underlying tissues (“blunt damage”). As the slant angle is increased, more scales enter in contact and distribute the force over a larger region of the substrate. This effect is very pronounced for the case $\alpha=75^\circ$, where scales tilt and contact in “domino effect” that involve about eight scales, distributing the puncture force over a large surface. Slanted scales can therefore improve the critical force of the system by distributing the force over a wider area.

4. Hard scales on a soft membrane: flexural compliance

In addition to resistance to puncture, flexural compliance is a desired property in scaled skin. In this section we used the DEM model to explore how the architecture of the scales affects flexural stiffness. In the model, a set of scales is perfectly bonded to a thin membrane of thickness h , depth b , and modulus E_m (Fig. 10a). The membrane was modeled with nonlinear co-rotational Euler-Bernoulli beam elements which assumed linear elasticity and small strains within the membrane, but allowed for arbitrarily large elemental rotations. The section of the membrane located below the rigid scales was also assumed to be rigid (Fig. 10a). In order to induce flexural deformations to the model, two self-equilibrated moments M were imposed at the ends of the membrane, inducing a state of pure bending. Fig. 10b shows the bending moment-curvature response for a membrane covered with cubic scales. Initially the flexural deformation of the thin membrane is the only contributor to the bending moment, so that the flexural stiffness is very low. As curvature increases the scales contact each other, which is characterized by an abrupt stiffening. In that second stage, the contact forces between the scales are balanced by tension in the membrane. These two forces create a couple which becomes the largest contributor to flexural stiffness. To better appreciate this mechanism we partitioned the total strain energy in the DEM model into the contributions from bending and axial strain energy in the membrane (Fig. 10c). In the initial stage the energy from axial stretch of the membrane is negligible compared to the energy from flexural deformation. After contact of the scales however, the energy from axial deformation increases dramatically.

To validate the flexural models we also fabricated and tested a membrane covered by ABS cubic scales (8mm×8mm×8mm). The scales were 3D-printed and glued onto a 1mm thick strip of polyurethane (Young’s modulus =4.5 MPa, measured in three-point bending). In the experiment, pure bending was induced in the membrane using a four-point bending configuration (Fig. 10d). Fig. 10b shows an excellent agreement between the experiment and the DEM model, except near the contact point. In the DEM model, contact is initiated simultaneously between all the scales which gives rise to a sharp transition in stiffness. In the experiments contact was initiated at slightly different deformation stage due to imperfections, which gave rise to a more progressive transition in the slope. We used the DEM approach to explore the effect of the scale geometry and arrangement on the flexural compliance of the scaled-membrane system. The moment was normalized according to classical beam theory as $M^*=Mt/E_m I_m$, and the curvature normalized as $\kappa^*=\kappa t$. Fig. 11 shows the effect of slant angle, scale length and scale gap. The normalized moment-curvature response followed the behavior described above: initially negligible stiffness, followed by rapid stiffening immediately after the scales enter contact. Interestingly, the post contact behavior shows softening, because the sliding of the contact points increase the moment arm on individual scales, effectively making the entire structure more compliant (softening is absent for cases with no slant, $\alpha=0$ because the contact points remain at the corner of the scales during the entire simulation). The deformation at which the scales contact, the amount of stiffening and softening depend largely on the geometric parameters. In addition, we observed that for designs with high slant angles, large scale size or small gap, the conformation induced a ‘zig-zagged’ deformation in the membrane.

Fig. 12 summarizes the flexural compliance for different combinations of gap sizes (d/t), aspect ratios (L/t) and slant angles (α). For all models, we considered a constant total membrane length of $L_{\text{whole}}/t = 100$. also, we put a limitation on loading where the system is

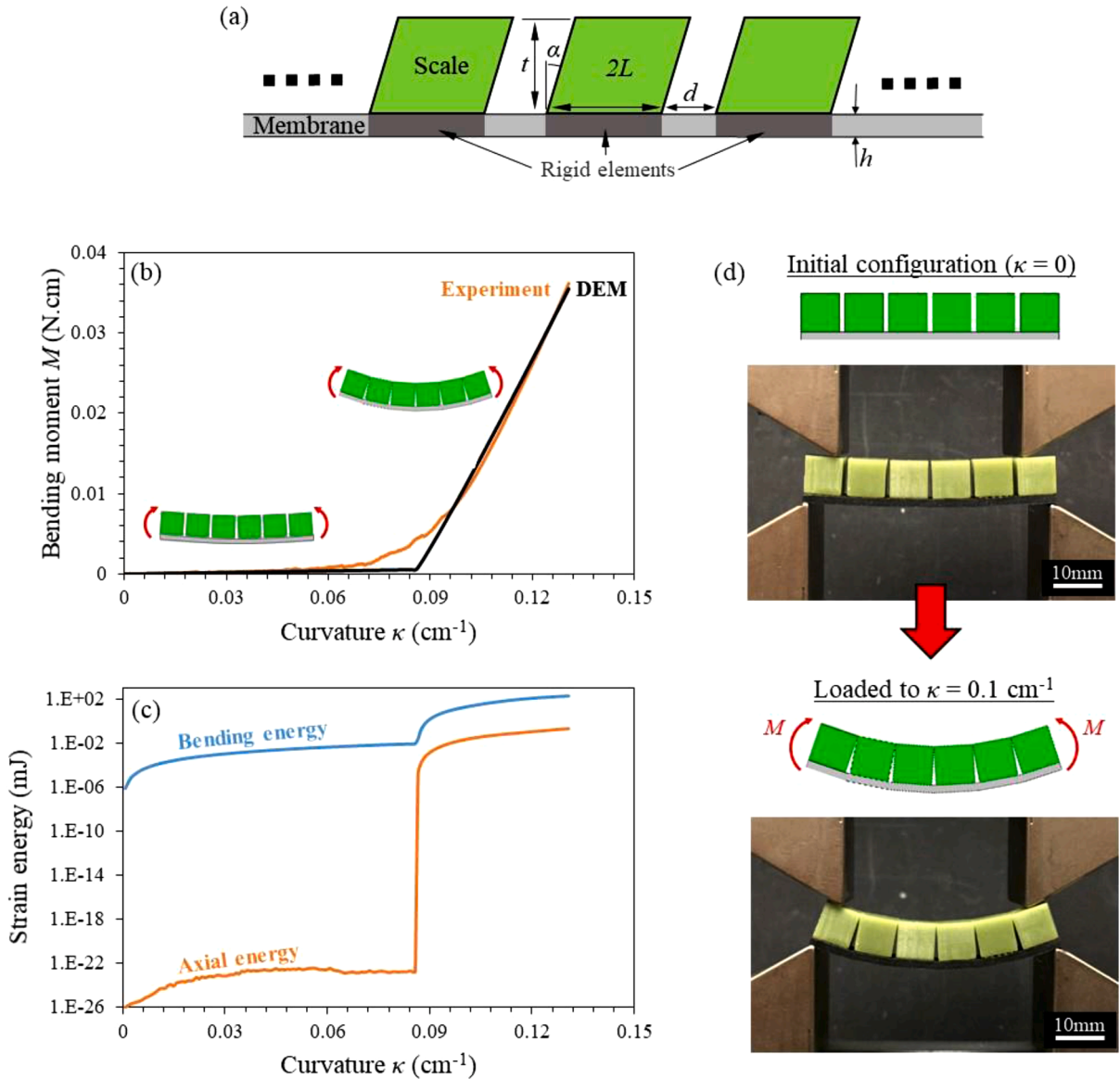


Fig. 10. (a) Schematic for the DEM flexural model; (b) Bending moment-curvature curves showing good agreement between the experiment and DEM results; (c) Evolution of strain energy from axial stresses and strain energy from bending stresses during loading, computed from the DEM simulations. (d) Comparison between a DEM simulation and an experiment on 3D printed blocks on elastomer strip.

loaded up to a maximum end rotation of 180°. In some designs, contact was never initiated in the simulation due to geometry (large gap sizes) and, therefore, were unaffected by the scale angle; these cases were plotted as unfilled dots in Fig. 12. Considering all other cases in which contact occurs during the loading (filled dots in Fig. 12), contact significantly decreases the flexural compliance of the system by up to three orders of magnitude. For small slant angles of $\alpha=0^\circ$ and $\alpha=30^\circ$, the highest flexural compliance is for the models with the smallest gap ($d/t=0.1$) and the smallest aspect ratio ($L/t=0.1$). For slant angles of $\alpha=60^\circ$ and $\alpha=75^\circ$, the highest flexural compliance is for the model with $d/t=0.5$, $L/t=0.1$, and the model with $d/t=1$, $L/t=0.1$, respectively. For the models with large slant angles, larger gaps therefore increased the flexibility to the system. Also, by increasing the aspect ratio of the scales the system gets stiffer, so smaller aspect ratios are desirable.

5. Optimum mechanical performance

From the previous sections, it is clear that several of the design parameters have conflicting effects on puncture resistance and flexural compliance. For example, increasing slant angle increases puncture resistance, but also decreases flexural compliance. In this section we seek designs which offer optimum combinations of four mechanical properties: (i) the coverage parameter λ (determined

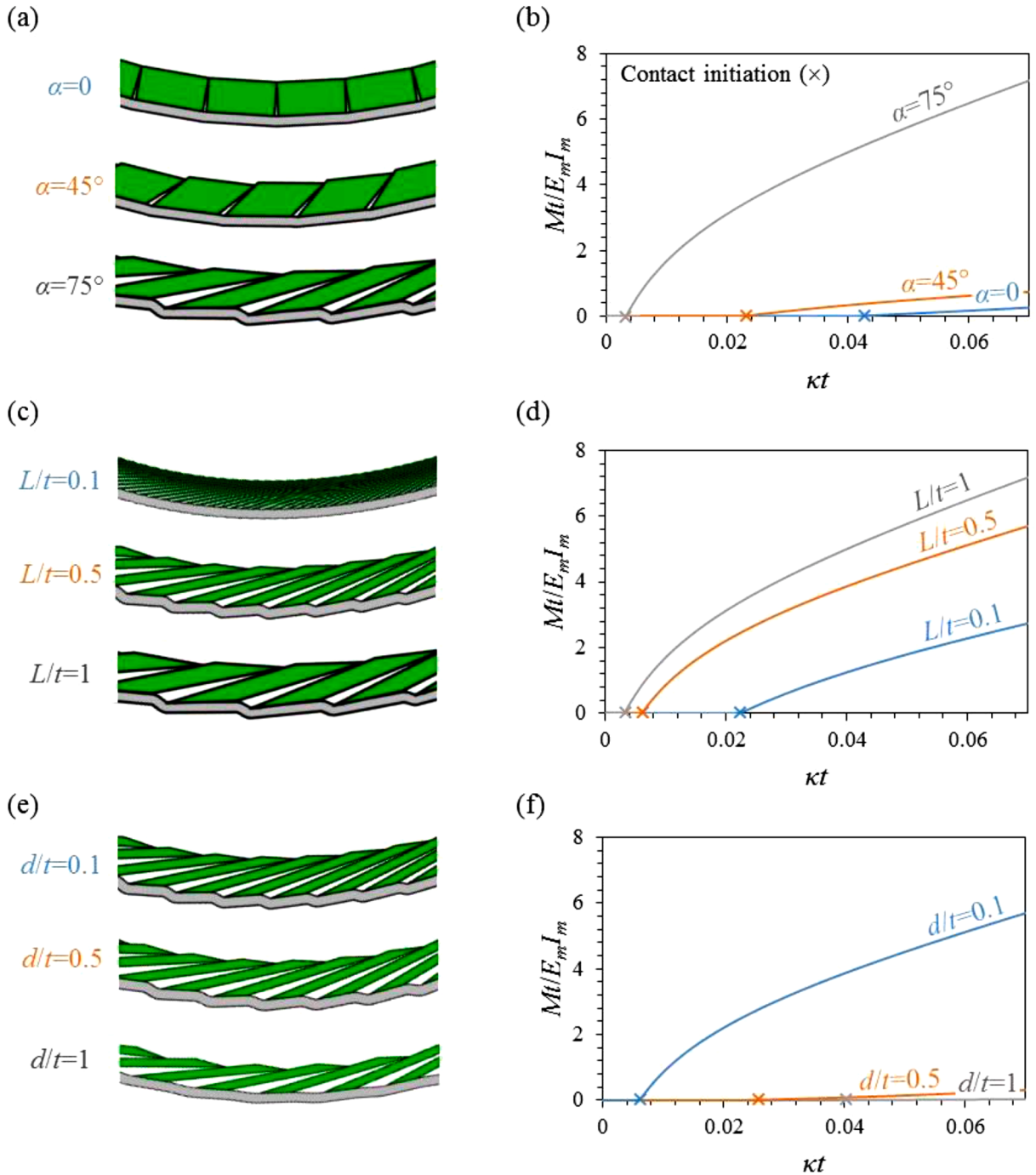


Fig. 11. Deformation of three systems of scales on a soft membrane under pure bending, and the related moment - curvature curves: for (a) and (b) a fixed aspect ratio of $L/t=1$ and a gap size of $d/t=0.1$, (c) and (d) a fixed gap size of $d/t=0.1$ and a slant angle of $\alpha=75^\circ$, and (e) and (f) a fixed aspect ratio of $L/t=0.5$ and a slant angle of $\alpha=75^\circ$.

using geometry, Fig. 5) (ii) the critical force (force at which the indented scale become mechanically instable), (iii) the penetration resistance (defined as the inverse of the maximum penetration of the scales into the substrate when the punctured scale reaches the critical tilting angle), (iv) the flexural compliance (defined as the inverse of the maximum slope in the moment-curvature curve). In order to find the best design, we parameterized the scale gap size $d/t = \{0.1, 0.2, \dots, 1\}$, aspect ratio $L/t = \{0.025, 0.05, 0.1, 0.2, \dots, 1\}$, and slant angle $\alpha = \{0^\circ, 15^\circ, \dots, 75^\circ\}$. We eliminated the designs where the coverage λ is zero, because these designs leave the substrate partially exposed to mechanical threats. We compared a set of models with various combinations of the three design parameters (the

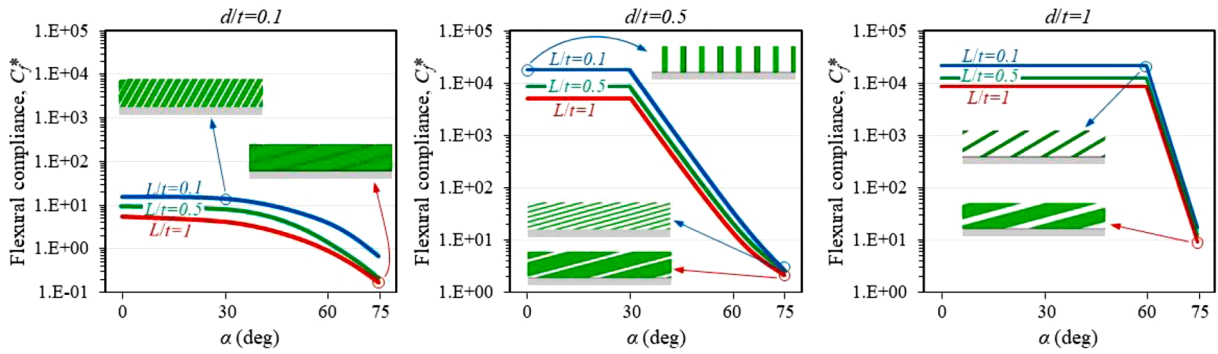


Fig. 12. The effect of the gap size, aspect ratio and slant angle on the flexural compliance of a series of scales on a soft membrane. The flexural compliance is denoted as C_f and normalized by $C_f^* = C_f E_m J_m$.

gap size, the aspect ratio and the slant angle) using a quaternary plot to find the best design for a given design performance criteria. As the four criteria have values with different orders of magnitude, we rescaled each criterion to a range from 0 to 1 in which the minimum and the maximum of each criterion are 0 and 1, respectively. We defined a fitness score as:

$$f = (Coverage)^m (Critical\ force)^n (Penetration\ resistance)^k (Flexural\ compliance)^l \tag{7}$$

The individual values of m , n , k and l can be tuned to control the influence of each criterion on the fitness score, but we required $m+n+k+l=1$. The best designs for any combinations of m , n , k and l can therefore be displayed on a quaternary plot, shown on Fig. 13. The corners of the tetrahedron shows the four designs that optimize one of the four criteria while the other three are ignored. High coverage ($m=1$) is obtained with small gap size, large aspect ratio and intermediate slant angle (45°). Maximum critical force ($n=1$) is obtained for small gap size, small aspect ratio and large slant angle. The best penetration resistance is obtained for a large gap size. Finally, the most flexible designs among the models ($l=1$) are achieved with scales with the smallest aspect ratio ($L/t = 0.025$) and a large slant angle ($\alpha = 60^\circ$). These four designs are very distinct, especially in terms of aspect ratio and gap distance. In order to identify the design with the best “balanced” set of properties, we sought the design that maximized f with $m=n=k=l=0.25$, to give equal weight to each performance metrics.

The design with the best balanced performance was $d/t=0.7$, $L/t=0.1$ and $\alpha=60^\circ$. Our approach also showed that this particular design dominates not only for $m=n=k=l=0.25$, but also for a wide variety of fitness parameters depicted by the orange volume on Fig. 13.

6. Summary

In this study we proposed the discrete element method to investigate the mechanical behaviour of systems of segmented scales attached to a soft substrate and a soft membrane. DEM is appropriate for this kind of system where the scales can be assumed to be rigid compared to the surrounding materials, and we validated the simulations with puncture and flexural experiments. The focus was to learn about the effect of the architecture (the aspect ratio and slant angle of the scales) and the arrangement (the gap size between the scales) of the scales on the mechanical performance of the scaled systems. The study gives us useful insights into the mechanics of this type of system, optimization of its mechanical performance, and eventually, a better design of synthetic fish-skin-like protective systems. The computational efficiency of DEM allows us to run a large number of nonlinear models (720 Models) with different combinations of the design parameters. To identify the best designs, we considered four criteria: critical force, coverage, penetration resistance and flexural compliance. The results show that the contact between the scales play a critical role in the behaviour of the system. The contact helps to distribute the load over a wider area therefore the system becomes more resistant to tilting and penetration. The main conclusions are as follow:

- The models with a high stiffness have a high critical force as well.
- The model with the highest critical force requires the smallest gap size and aspect ratio, and the largest slant angles.
- The smallest gap size, the largest aspect ratio and a moderate slant angle of 45° give the best coverage.
- Contact makes the force distribution occur over a wider area which results in a higher critical force and penetration resistance. On the other hand, too many contact points has negative effects on the penetration resistance.
- To have the highest flexural compliance the aspect ratio needs to be the smallest.
- There is limitation on the positive effect of the slant angle on the flexural compliance: too large slant angle decreases the flexibility of the system.

We used a quaternary plot to examine the influence of the design parameters (gap size, aspect ratio and slant angle) on the four mechanical properties: coverage, critical force, penetration resistance and flexural compliance. The quaternary plot shows that changing each design parameter can improve one mechanical property while having a negative effect on the other ones. Also, based on

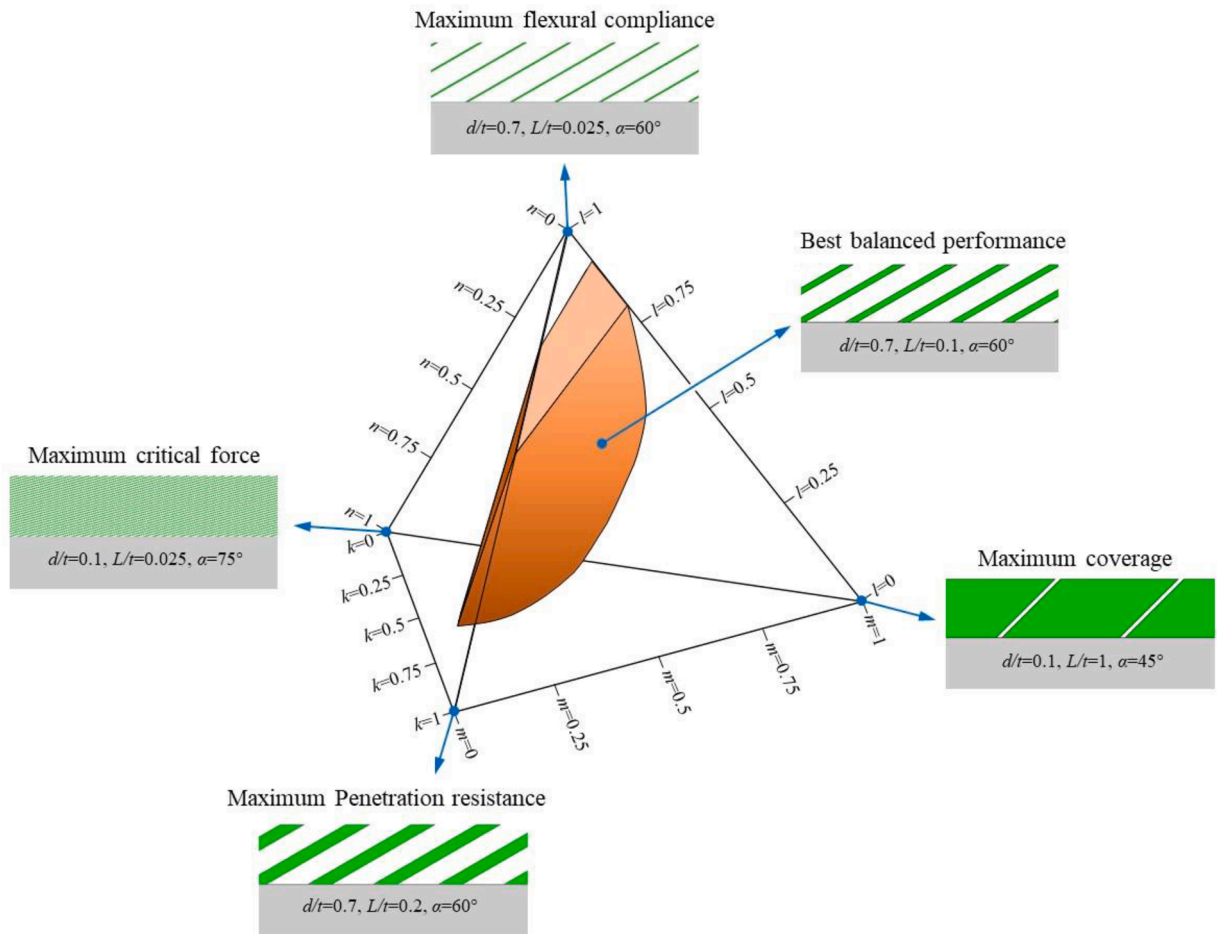


Fig. 13. The quaternary plot showing the best designs for the fitness indices of $m=1$, $n=1$, $k=1$ and $l=1$ (the four corners of the plot). Also the best balanced design is shown for the case with $(m=0.25, n=0.25, k=0.25, l=0.25)$.

which mechanical properties are more important to be considered, we give a weight to each criterion (m , n , k and l), which results in different combinations of design parameters. The best response of the system considering the four criteria with the equal weights ($m=0.25$, $n=0.25$, $k=0.25$ and $l=0.25$) belongs to the model with a small aspect ratio ($L/t=0.1$), intermediate gap size ($d/t=0.7$) and large slant angle ($\alpha=60^\circ$). This article provides a strong basis for future design of synthetic fish-skin-like protective systems. Further simulations would be needed to optimize the design parameters for specific applications and boundary conditions, and could include material nonlinearity in the substrate for better accuracy at large deformations. Adding nonlinearities and unusual behavior to the substrate could indeed enrich the problem and possibly lead to new and interesting interactions between the scales and the substrate. The focus on this DEM-based method is on systems where the scales are orders of magnitude stiffer than the substrate, which is relevant for many types of flexural armor (biological and engineered). For the cases where the deformation of individual scales cannot be neglected, other numerical approaches such as finite elements must be used. Finite element is however much more expensive computationally because of contact penalty methods and much greater number of degrees of freedom.

CRediT authorship contribution statement

Ali Shafiei: Conceptualization, Methodology, Software, Validation, Formal analysis, Investigation, Writing - original draft, Visualization. **J. William Pro:** Conceptualization, Methodology, Software, Formal analysis, Writing - original draft. **Roberto Martini:** Conceptualization, Methodology, Formal analysis, Investigation. **Francois Barthelat:** Conceptualization, Methodology, Investigation, Resources, Writing - review & editing, Supervision, Project administration, Funding acquisition.

Declaration of Competing Interest

We declare that there are no conflicts of interest regarding our submission entitled “The very hard and the very soft: Modeling bio-inspired scaled skins using the discrete element method”, by Ali Shafiei, J. William Pro, Roberto Martini, and Francois Barthelat.

Acknowledgments

This work was supported by a Discovery Grant from the Natural Sciences and Engineering Research Council of Canada. A.S. was partially supported by a McGill Engineering Doctoral Award.

References

- Abid, N., Mirkhalaf, M., Barthelat, F., 2018. Discrete-element modeling of nacre-like materials: Effects of random microstructures on strain localization and mechanical performance. *J. Mech. Phys. Solids* 112, 385–402.
- Abid, N., Pro, J.W., Barthelat, F., 2019. Fracture mechanics of nacre-like materials using discrete-element models: effects of microstructure, interfaces and randomness. *J. Mech. Phys. Solids* 124, 350–365.
- Barber, J.R., 2002. *Elasticity*. Springer.
- Barthelat, F., 2015. Architected materials in engineering and biology: fabrication, structure, mechanics and performance. *Int. Mater. Rev.* 60 (8), 413–430.
- Bolander, J.E., Saito, S., 1998. Fracture analyses using spring networks with random geometry. *Eng. Fract. Mech.* 61 (5), 569–591.
- Browning, A., Ortiz, C., Boyce, M.C., 2013. Mechanics of composite elasmoid fish scale assemblies and their bioinspired analogues. *J. Mech. Behav. Biomed. Mater.* 19, 75–86.
- Burger, J., Zappalorti, R.T., 2011. *The Northern Pine Snake (Pituophis melanoleucus) its Life History, Behavior and Conservation*. Nova Science Publishers, Inc., New York.
- Chen, I.H., Kiang, J.H., Correa, V., Lopez, M.I., Chen, P.Y., McKittrick, J., Meyers, M.A., 2011. Armadillo armor: mechanical testing and micro-structural evaluation. *J. Mech. Behav. Biomed. Mater.* 4 (5), 713–722.
- Chintapalli, R.K., Mirkhalaf, M., Dastjerdi, A.K., Barthelat, F., 2014. Fabrication, testing and modeling of a new flexible armor inspired from natural fish scales and osteoderms. *Bioinspirat. Biomimet.* 9 (3).
- Chintapalli, R.K., Mirkhalaf, M., Dastjerdi, A.K., Barthelat, F., 2014. Fabrication, testing and modeling of a new flexible armor inspired from natural fish scales and osteoderms. *Bioinspiration Biomimetics* 9 (3), 036005.
- Connors, M., Yang, T., Hosny, A., Deng, Z., Yazdandoost, F., Massaadi, H., Eernisse, D., Mirzaeifar, R., Dean, M.N., Weaver, J.C., Ortiz, C., Li, L., 2019. Bioinspired design of flexible armor based on chiton scales. *Nat. Commun.* 10 (1), 5413.
- Dugué, M., Fivel, M., Bréchet, Y., Dendievel, R., 2013. Indentation of interlocked assemblies: 3D discrete simulations and experiments. *Comput. Mater. Sci.* 79, 591–598.
- Funk, N., Vera, M., Szewciw, L.J., Barthelat, F., Stoykovich, M.P., Vernerey, F.J., 2015. Bioinspired Fabrication and Characterization of a Synthetic Fish Skin for the Protection of Soft Materials. *ACS Appl. Mater. Interfaces* 7 (10), 5972–5983.
- Garst, W., Garst, G.S., 1985. *Warren and Genevieve Garst Photographic Collection*. Colorado State University.
- Johnson, K.L., 1987. *Contact Mechanics*. Cambridge university press.
- Li, M., Dai, M., 2020. A simple method for spherical indentation of an elastic thin layer with surface tension bonded to a rigid substrate. *Appl. Math. Modell.* 81, 653–662.
- Lim, R.K., Pro, J.W., Begley, M.R., Utz, M., Petzold, L.R., 2015. High-performance simulation of fracture in idealized ‘brick and mortar’ composites using adaptive Monte Carlo minimization on the GPU. *Int. J. High Perform. Comput. Appl.* 30 (2), 186–199.
- Lin, Y.-Y., Chang, C.-F., Lee, W.-T., 2008. Effects of thickness on the largely-deformed JKR (Johnson–Kendall–Roberts) test of soft elastic layers. *Int. J. Solids Struct.* 45 (7), 2220–2232.
- Martini, R., Balit, Y., Barthelat, F., 2017. A comparative study of bio-inspired protective scales using 3D printing and mechanical testing. *Acta Biomater.* 55, 360–372.
- Martini, R., Barthelat, F., 2016. Stability of hard plates on soft substrates and application to the design of bioinspired segmented armor. *J. Mech. Phys. Solids* 92, 195–209.
- Martini, R., Barthelat, F., 2016. Stretch-and-release fabrication, testing and optimization of a flexible ceramic armor inspired from fish scales. *Bioinspirat. Biomimet.* 11 (6), 066001.
- O. Nelson, *Illinois Gar Summit I*. <<http://moxostoma.com/illinois-gar-summit-i-feb-2014/>>, 2014).
- okumura, I.A., 1995. On the generalization of cerruti’s problem in an elastic half-space. *Doboku Gakkai Ronbunshu* 1995 (519), 1–10.
- Porter, M.M., Novitskaya, E., Castro-Ceseña, A.B., Meyers, M.A., McKittrick, J., 2013. Highly deformable bones: Unusual deformation mechanisms of seahorse armor. *Acta Biomater.* 9 (6), 6763–6770.
- Pro, J.W., Barthelat, F., 2019. Discrete element models of tooth enamel, a complex three-dimensional biological composite. *Acta Biomater.* 94, 536–552.
- Pro, J.W., Barthelat, F., 2020. Discrete element models of fracture in tooth enamel: Failure mode competition and statistical effects. *J. Mech. Phys. Solids* 137, 103868.
- Pro, J.W., Lim, R.K., Petzold, L.R., Utz, M., Begley, M.R., 2015. The impact of stochastic microstructures on the macroscopic fracture properties of brick and mortar composites. *Extreme Mech. Lett.* 5, 1–9.
- Pro, J.W., Lim, R.K., Petzold, L.R., Utz, M., Begley, M.R., 2015. GPU-based simulations of fracture in idealized brick and mortar composites. *J. Mech. Phys. Solids* 80, 68–85.
- Rajabi, H., Shafiei, A., Darvizeh, A., Dirks, J.-H., Appel, E., Gorb, S.N., 2016. Effect of microstructure on the mechanical and damping behaviour of dragonfly wing veins. *R. Soc. Open Sci.* 3 (2), 160006.
- Rajabi, H., Shafiei, A., Darvizeh, A., Gorb, S.N., 2016. Resilin microjoints: a smart design strategy to avoid failure in dragonfly wings. *Sci. Rep.* 6, 39039.
- Ritchie, R.O., 2011. The conflicts between strength and toughness. *Nat. Mater.* 10 (11), 817–822.
- Rudykh, S., Ortiz, C., Boyce, M.C., 2015. Flexibility and protection by design: imbricated hybrid microstructures of bio-inspired armor. *Soft Matter* 11 (13), 2547–2554.
- Vernerey, F.J., Barthelat, F., 2010. On the mechanics of fishscale structures. *Int. J. Solids Struct.* 47 (17), 2268–2275.
- Vernerey, F.J., Barthelat, F., 2014. Skin and scales of teleost fish: Simple structure but high performance and multiple functions. *J. Mech. Phys. Solids* 68, 66–76.
- Vernerey, F.J., Musiket, K., Barthelat, F., 2014. Mechanics of fish skin: A computational approach for bio-inspired flexible composites. *Int. J. Solids Struct.* 51 (1), 274–283.
- Wegst, U.G.K., Bai, H., Saiz, E., Tomsia, A.P., Ritchie, R.O., 2014. Bioinspired structural materials. *Nat. Mater.* 14, 23.
- Wu, J., Ru, C.Q., 2019. Spherical indentation of an elastic layer on a rigid substrate revisited. *Thin Solid Films* 669, 500–508.
- Yang, W., Chen, I.H., Gludovatz, B., Zimmermann, E.A., Ritchie, R.O., Meyers, M.A., 2013. Natural Flexible Dermal Armor. *Adv. Mater.* 25 (1), 31–48.
- Zhu, D.J., Ortega, C.F., Motamedi, R., Szewciw, L., Vernerey, F., Barthelat, F., 2012. Structure and Mechanical Performance of a “Modern” Fish Scale. *Adv. Eng. Mater.* 14 (4), B185–B194.
- Zhu, D.J., Szewciw, L., Vernerey, F., Barthelat, F., 2013. Puncture resistance of the scaled skin from striped bass: Collective mechanisms and inspiration for new flexible armor designs. *J. Mech. Behav. Biomed. Mater.* 24, 30–40.